ADVANCES IN ATMOSPHERIC SCIENCES, VOL. 29, NO. 3, 2012, 529–543

The Tropical Intraseasonal Oscillation in SAMIL Coupled and Uncoupled General Circulation Models

YANG Jing[1] (杨 静), BAO Qing*[2] (包 庆), WANG Xiaocong[2] (王晓聪), and ZHOU Tianjun[2] (周天军)

[1]*State Key Laboratory of Earth Surface Processes and Resource Ecology, Beijing Normal University, Beijing* 100875

[2]*State Key Laboratory of Numerical Modeling for Atmospheric Sciences and Geophysical Fluid Dynamics, Institute of Atmospheric Physics, Chinese Academy of Sciences, Beijing* 100029

(Received 21 June 2011; revised 19 November 2011)

ABSTRACT

Simulations of tropical intraseasonal oscillation (TISO) in SAMIL, the Spectral Atmospheric Model from the Institute of Atmospheric Physics (IAP) State Key Laboratory of Numerical Modeling for Atmospheric Sciences and Geophysical Fluid Dynamics (LASG) coupled and uncoupled general circulation models were comprehensively evaluated in this study. Compared to the uncoupled model, the atmosphere–ocean coupled model improved the TISO simulation in the following aspects: (1) the spectral intensity for the 30–80-day peak eastward periods was more realistic; (2) the eastward propagation signals over western Pacific were stronger; and (3) the variance distribution and stronger signals of Kelvin waves and mixed Rossby gravity waves were more realistic. Better performance in the coupled run was assumed to be associated with a better mean state and a more realistic relationship between precipitation and SST. In both the coupled and uncoupled runs, the unrealistic simulation of the eastward propagation over the equatorial Indian Ocean might have been associated with the biases of the precipitation mean state over the Indian Ocean, and the unrealistic split of maximum TISO precipitation variance over the Pacific might have corresponded to the exaggeration of the double Intertropical Convergence Zone (ITCZ) structure in precipitation mean state. However, whether a better mean state leads to better TISO activity remains questionable. Notably, the northward propagation over the Indian Ocean during summer was not improved in the mean lead–lag correlation analysis, but case studies have shown some strong cases to yield remarkably realistic northward propagation in coupled runs.

Key words: tropical intraseasonal oscillation, atmosphere-ocean interaction, mean state, northward propagation, simulation

Citation: Yang, J., Q. Bao, X. C. Wang, and T. J. Zhou, 2012: The tropical intraseasonal oscillation in SAMIL coupled and uncoupled general circulation models. *Adv. Atmos. Sci.*, **29**(3), 529–543, doi: 10.1007/s00376-011-1087-3.

1. Introduction

The tropical intraseasonal oscillation (TISO) is an important element of the tropical atmospheric climate system. The most dominant component of TISO during winter is the eastward propagating Madden-Julian Oscillation (MJO, Madden and Julian, 1971, 1972). During summer, the MJO disturbances weaken and TISO additionally involves a prominent northward propagation (Krishnamurti and Subrahmanyam, 1982; Murakami et al., 1984; Lau and Chan, 1986; Wang and Rui, 1990; Yang et al., 2008; among many others). The significant role of TISO on our weather and climate systems has been widely recognized. TISO has been intimately associated with the onsets and breaks of the monsoon systems (e.g., Yasunari, 1979; Hendon and Liebmann, 1990; Zhou and Chan, 2005), the formation of tropical cyclones (e.g., Liebmann et al., 1994; Maloney and Hartmann, 2000; Higgins and Shi, 2001), the triggering or termination of some El Niño

*Corresponding author: BAO Qing, baoqing@mail.iap.ac.cn.

events (e.g., Takayabu et al., 1999; Kessler and Kleeman, 2000; Bergman et al., 2001), and the modulation of the biological and chemical components (e.g., chlorophyll: Waliser et al., 2005; ozone: Tian et al., 2007; aerosols: Tian et al., 2008). Being a strong tropical heating source, the TISO also influences the extratropics by driving teleconnection (e.g., Weickmann, 1983; Liebmann and Hartmann, 1984, Pan and Li, 2008). Hence, a realistic simulation of TISO is necessary for the accurate simulation and skillful prediction of weather and climate phenomena.

Unfortunately, poor simulation of the TISO is a fairly generic problem in general circulation models (GCMs). Typical errors in climate models include a weak amplitude, periods that are too short, eastward propagation during winter that are too fast, northward propagation during summer that is too weak (e.g., Hayashi and Golder, 1986; Lau et al., 1988; Slingo et al., 1996; Sperber et al., 1997; Fu and Wang, 2004). TISO essentially involves the complex interactions between convection and large-scale dynamics, together with the interactions between the sea surface and the boundary layer (Wang, 2005). Accordingly, TISO modeling problems have been associated with inadequate representation of the following aspects: moisture convection (e.g., Tokioka et al., 1988; Wang and Schlesinger, 1999; Zhang and Song, 2009), stratiform rainfall (Fu and Wang, 2009; Kim et al., 2009), the vertical profile of heating (Jiang et al., 2009; Li et al., 2009), the mean state (Wang and Xie, 1997; Inness et al., 2003; Ajayamohan and Goswami, 2007, among many others), and the atmosphere–ocean interaction (e.g., Wang and Xie, 1998; Waliser et al., 1999; Hendon, 2000; Fu and Wang, 2004; Sperber et al., 2005, among many others).

Recently, in preparation for the Intergovernmental Panel on Climate Change (IPCC) Fifth Assessment Report (AR5), the atmospheric component (SAMIL: Spectral Atmospheric Model in IAP/LASG) of the IAP coupled model FGOALS-s (the Flexible Global Ocean–Atmosphere–Land System model) made several modifications of the physical parameterization package, including radiation scheme, convective parameterization scheme, and cloud scheme (Bao et al., 2010). Before conducting the extended simulations of different climate change scenarios, this model performed both AMIP (Atmospheric Model Intercomparison Project) and CMIP (Coupled Model Intercomparison Project) (Taylor et al., 2009) runs. Moreover, it is of interest to assess respective TISO simulations in this new generation of the climate model to examine the effects of both the updated physical processes and atmosphere–ocean coupling on TISO simulation. Such an evaluation is also important for evaluating the general performance of this climate model in terms of its use regarding climate change projections in the IPCC AR5.

The model, the validation data, and the methodology are introduced in section 2. In section 3, the basic performance of TISO simulation (including power spectrum, propagation and geographic distribution) are described, and in section 4 the impact of atmosphere–ocean interaction and mean state on simulation of TISO is discussed. Conclusions derived from this study are listed in the last section.

2. Model, validation data, and methodology

2.1 *The model*

The atmospheric component of FGOALS-s is version 2.4.7 of SAMIL (Bao et al., 2010), a spectral transform model with 26 atmospheric layers extending from the surface to 2.19 hPa, and with a horizontal resolution of R42 [$\sim$2.81° (longitude) $\times$1.66° (latitude)]. The time increment of integration in the current version of SAMIL R42L26 is 10 minutes. The radiation scheme is the Edwards-Slingo scheme from the UK Meteorological Office (Edwards and Slingo, 1996), with a modification by Sun (Sun and Rikus, 1999a, b). The time step of the radiation scheme is 1 hour, indicating that the diurnal cycle of solar radiation can be captured. The mass flux cumulus parameterization of Tiedtke (Tiedtke, 1989) is utilized for representing the deep, shallow and midlevel convections, with a modified closure assumption and the formation of organized entrainment and detrainment (Nordeng, 1994; Song, 2005). The planetary boundary layer (PBL) part of the model is a higher-order closure scheme that computes the turbulent transfer of momentum, heat, moisture, and cloud water (Brinkop and Roeckner, 1995). The cloud scheme is a diagnostic method based on vertical motion and relative humidity (Liu and Wu, 1997). The effects of gravity-wave drag are also considered, which depend on wind speed, density, and static stability of the low-level flow (Palmer, 1996). The oceanic component is LASG IAP Common Ocean Model (LICOM) (Liu et al., 2004), and its resolution is 1°$\times$1° with the increased resolution to 0.5°$\times$0.5° in tropical regions.

In AMIP, the observed SST and sea ice temperature from 1979 to 2008 served as the boundary forcing of numerical experiments. And the realistic forcing of greenhouse gas, solar constant and aerosol were also used to conduct standard AMIP runs for the period 1979–2008. The CMIP historical run performed the integration for 1850–2005, with realistic external forcing including greenhouse gas, solar radiation, ozone

distribution, and aerosols. To facilitate the comparison with observation data, the 11-year results from 1991 to 2001 in the model were used in this study.

2.2 *Validation data and methodology*

We validated the simulations against to the daily and monthly rainfall data retrieved from the Global Precipitation Climatology Project (GPCP, Huffman et al., 2001), and the daily and monthly upper and lower tropospheric winds data from NCEP/NCAR reanalysis (Kalnay et al., 1996). The records of 11 years (1998–2008) were applied in this study.

The U.S. Climate Variability Research Program (US CLIVAR) established the Madden-Julian Oscillation Working Group (MJOWG), which has developed a standardized set of diagnostics to evaluate MJO simulation in climate models (CLIVAR MJOWG 2008, http://www.usclivar.org/mjo.php). The MJOWG encourages the modeling community to apply this hierarchy of diagnostics to their simulations to allow for a systematic comparison with other models. These methodologies have been introduced in detail by Waliser et al. (2009) and Kim et al. (2009). In this study, we applied these diagnostics to climate model simulations. The boreal winter was defined from November to April (NOV–APR), and the boreal summer was from May to October (MAY–OCT). The 20–100-day band-pass filtered anomalies were constructed using a 201-point Lanczos filter (Duchon, 1979), which has half-power points at 20- and 100-day periods.

3. Simulation of TISO

3.1 *Power spectrum*

We used an equatorial wavenumber-frequency diagram (Hayashi, 1979) of daily time series of precipitation and 850-hPa zonal wind (U850) to isolate the characteristic spatial and temporal scales (Fig. 1). Consistent with previous results (e.g., Weickmann et al., 1985; Kiladis and Weickmann, 1992; Zhang et al., 2006), the dominant spatial scale according to observation data were zonal wavenumbers 1 to 3 for precipitation (Fig. 1a) and for U850 the dominant spatial scale was zonal wavenumber 1 for eastward periods of 30–80 days (Fig. 2a). These features were distinguishable in both summer and winter.

In AMIP (Figs. 1b and 2b), the zonal wavenumbers 1–3 of precipitation and the zonal wave number 1 of U850 in eastward propagating power were captured in some degree during both winter and summer. However, the spectral intensities during westward periods were unrealistically overestimated in both U850 and precipitation. The 30–80-day peak during eastward periods failed to appear in both precipitation and U850 during winter and summer. And the eastward propagating power tended to be concentrated at a lower frequency (period >80 days) and at a higher frequency (period <30 days).

In contrast, as shown in Figs. 1c and 2c, the CMIP generally enhanced the spectral power of 30–80-day eastward periods and reduced the powers at periods <30 days and <80 days, although the power of 30–80-day periods was weaker compared to the observation data. Meanwhile, the eastward propagating signals were strengthened relative to the westward propagating signals for both U850 and precipitation in winter in CMIP.

Additionally, wavenumber-frequency spectra (Wheeler and Kiladis, 1999) showed that the signals of Kelvin and equatorial Rossby wave were weaker in both CMIP and AMIP compared to the observation data (Figs. 3a–c). However, the signals of the equatorial Kelvin wave and the mixed Rossby gravity wave (MRG) were remarkably stronger in CMIP than in AMIP (Figs. 3a–c).

3.2 *Propagation*

3.2.1 *Eastward propagation*

In Fig. 4a, the eastward propagation of the TISO is shown by a lagged-time-longitude diagram of correlation coefficients between 20–100-day filtered precipitation and U850 along the equator (10°S–10°N) upon the 20–100-day filtered precipitation over the Indian Ocean (10°S–5°N, 75°–100°E, the reference region). TISO propagated eastward from the Indian Ocean to the western Pacific Ocean, with a typical phase speed of $\sim$5 m s^{-1} according to the observation data. Precipitation and U850 tended to be in quadrature, with the maximum precipitation leading the 850-hPa westerly wind. This results exhibit the classic MJO structure described first by Madden and Julian (1972).

In AMIP (Fig. 4b), the eastward propagation of U850 was detectable over the western Pacific Ocean but disappeared over the Indian Ocean in winter. In summer, the eastward propagation was, to some extent, represented over the Indian Ocean portion but was too weak to be detected over the western Pacific Ocean. The quadrature relationship between precipitation and U850 was reproducible over the Indian Ocean and the western Pacific Ocean in summer, but it was less well represented in winter. The CMIP strengthened the eastward propagating signals in the western Pacific Ocean during both summer and winter (Fig. 4c).

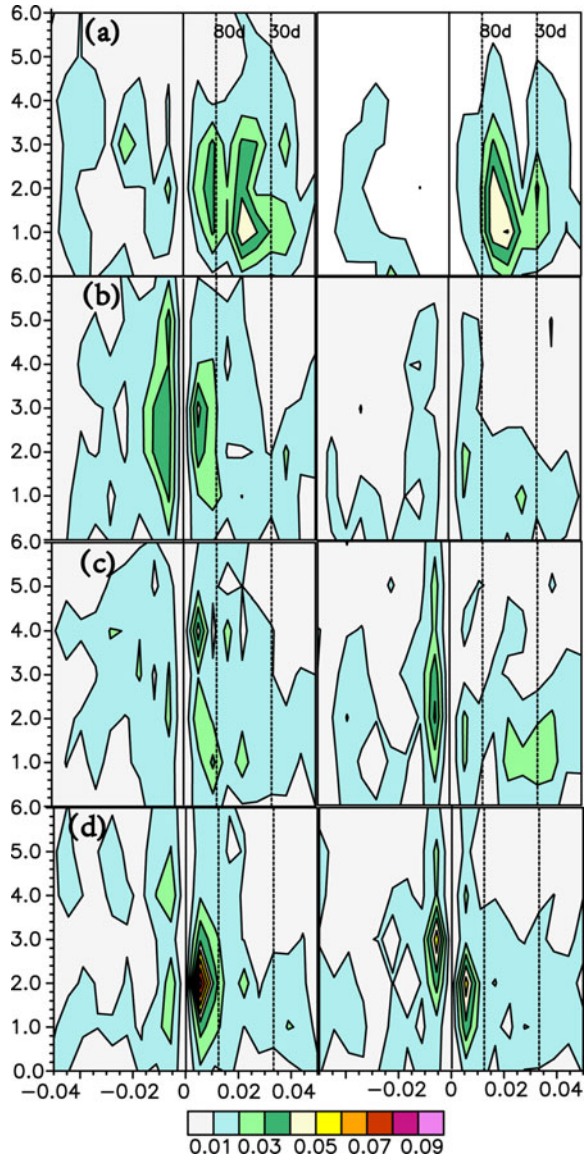

Fig. 1. Wavenumber-frequency spectra of precipitation averaged over 10°S–10°N during boreal winter (left) and summer (right), respectively in (a) observation data, (b) AMIP, (c) CMIP, and (d) AMIP-CMIP_SST. Individual spectra were calculated year by year before they were averaged in 11 years. The climatologically seasonal mean was removed before calculation of spectra. Units for the precipitation spectrum are $mm^2\ d^{-2}$. The bandwidth is $(180\ d)^{-1}$.

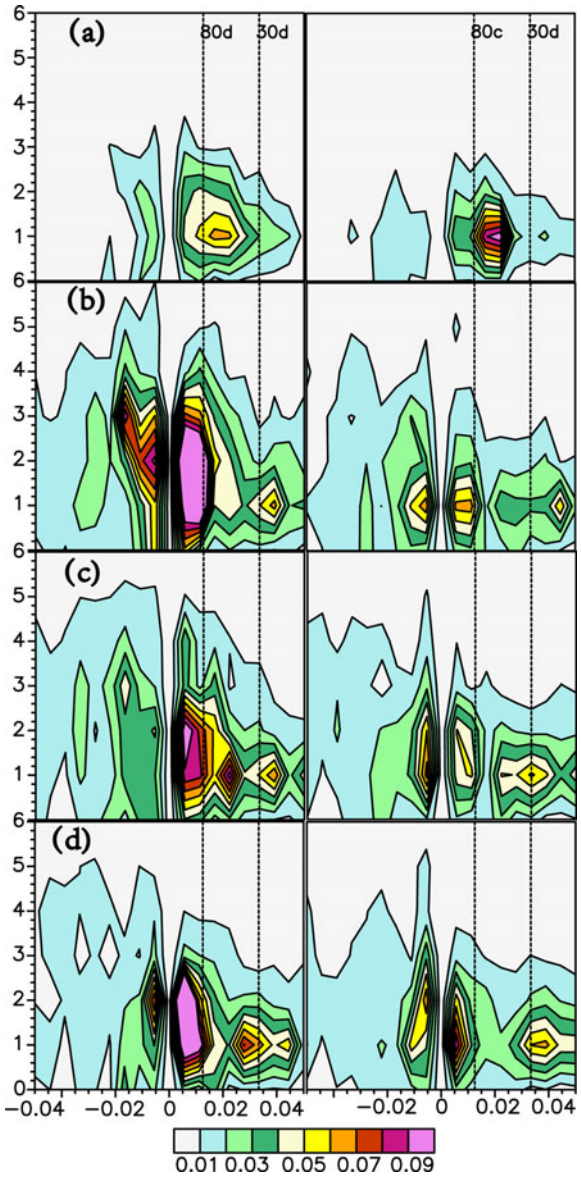

Fig. 2. The same as Fig. 1 except for the U850. The units are $m^2\ s^{-2}$.

3.2.2 *Northward propagation in summer*

Many previous studies (e.g., Krishnamurti and Subrahmanyam, 1982; Lau and Chan, 1986; Wang and Rui, 1990; among many others) have noted the evident continuous northward propagation of TISO from the equator to 20°N during summer according to the observation data (Fig. 5a), which was not realistically represented in both AMIP and CMIP (Figs. 5b and c). In AMIP, the northward propagating signal only occurred from 15°N to 25°N in the off-equatorial region. However, the northward propagation almost disappeared in CMIP. This result that seems to conflict with some previous studies, which showed that atmosphere–ocean interaction strengthens the northward propagation (e.g., Wang and Xie, 1998; Waliser et al., 1999; Hendon, 2000; Fu and Wang, 2004; Sperber et al., 2005, among many others). The quadrature relationship between precipitation and U850 according to the observation data was detected in both AMIP and CMIP.

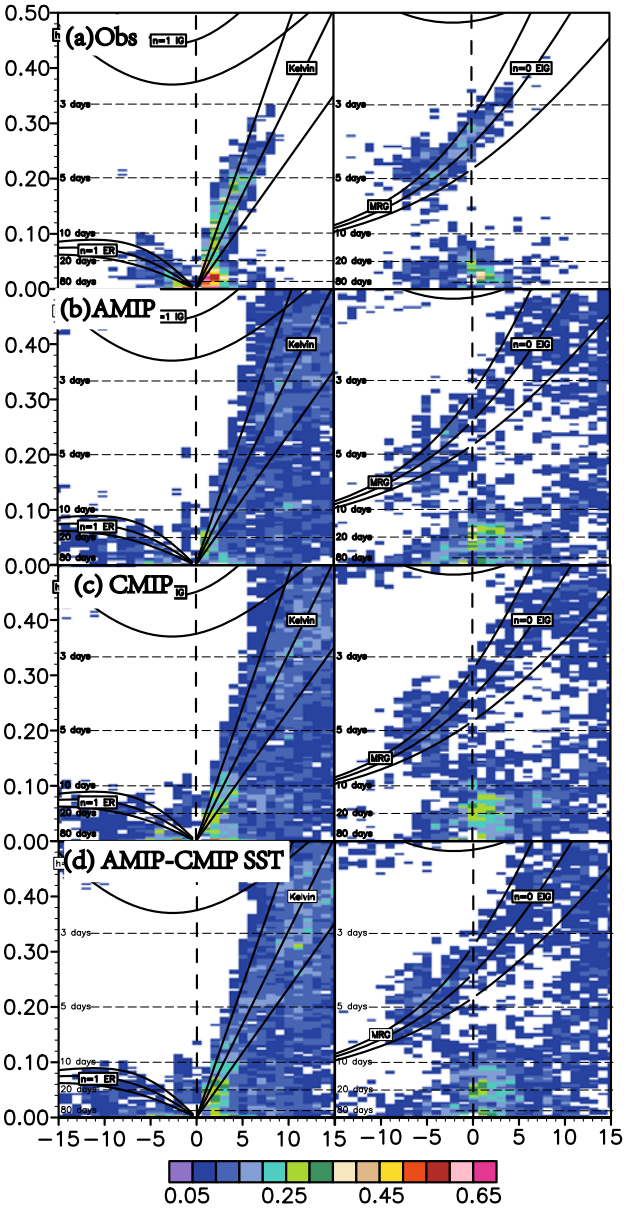

Fig. 3. The symmetric (left panel) and asymmetric (right panel) spectrum of coherence squared (color shading) between rainfall and U850, respectively in (a) observation data, (b) AMIP, (c) CMIP, and (d) AMIP-CMIP-SST. Spectra were computed for individual latitudes before they were averaged over 15°S–15°N. Computations were conducted using data in all seasons on 256-day segments, overlapping by 206 days. Dispersion curves are shown for the Kelvin, equatorial Rossby (ER), eastward intertio-gravity (EIG), and mixed Rossby–gravity (MRG) modes.

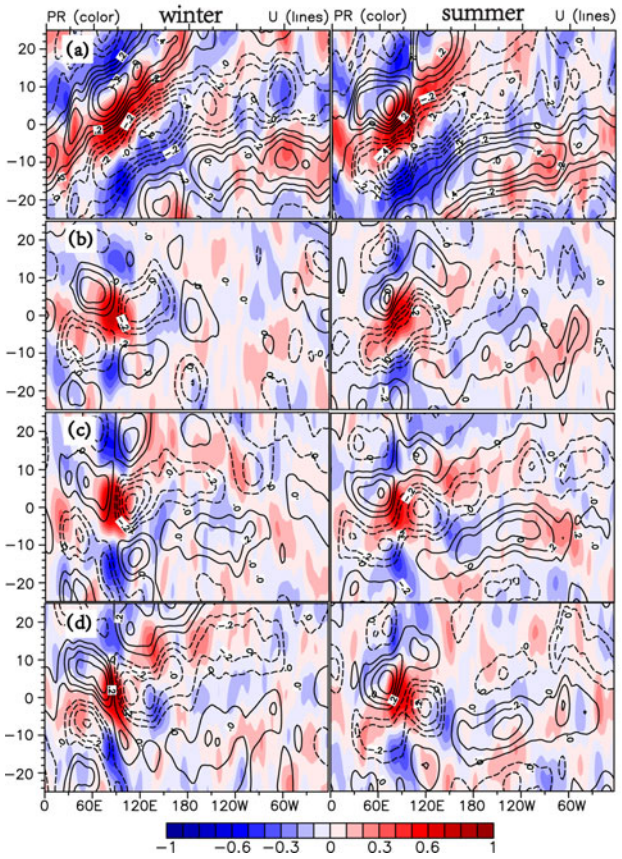

Fig. 4. Lagged-time-longitude diagram of correlation coefficients between the 20–100-day band-pass filtered precipitation (color shadings) and the U850 (contours) over 10°S–10°N during boreal winter (left) and boreal summer (right) compared to the 20–100-day filtered precipitation over the reference region (10°S–5°N and 75°–100°E), respectively for (a) observation data, (b) AMIP, (c) CMIP, and (d) AMIP-CMIP_SST. Contour interval is 0.1. The absolute value > 0.2 is above the 95% confidence level.

3.3 *Geographic distribution*

To investigate how the magnitude and geographical distribution of 20–100-day TISO were simulated, we examined the maps of the 20–100-day filtered variance for both U850 and precipitation (Fig. 6). During winter, the U850 and precipitation variance maxima were located over the eastern Indian Ocean, the western Pacific Oceanth, and south of the Maritime continent region, according to the observation data (Fig. 6a). The three maxima centers were approximately detected in both AMIP and CMIP, but the amplitudes of variance were generally overestimated in both simulations (Figs. 6b and c). In AMIP, the amplitude of the variance maxima over the western Pacific Ocean was obviously overestimated; and the maximum center of variance over the Indian Ocean shifted southwestward. In CMIP, the location of U850 and the precipitation variance maxima, over the central tropical Indian Ocean, was obviously nearer to the observation data than in AMIP. Meanwhile, the amplitude over the western Pacific Ocean in CMIP was more realistic

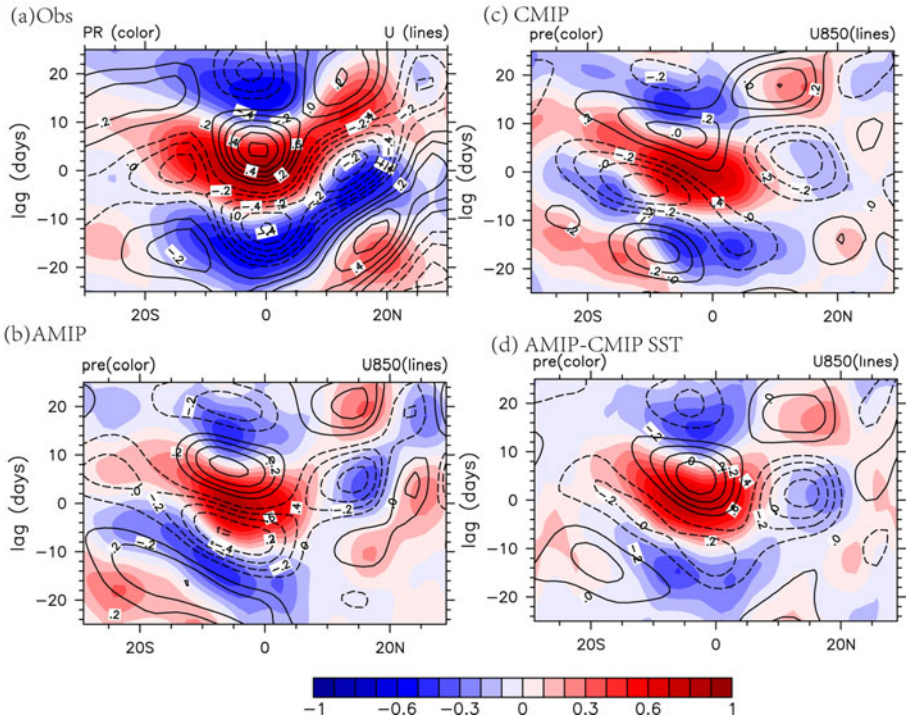

Fig. 5. Lagged-time-latitude diagram of correlation coefficients between 20–100-day band-pass filtered precipitation (color shadings) and U850 (contours) over 75°–100°E during boreal summer against to the 20–100-day filtered precipitation over the reference region (5°N–10°S and 75°–100°E), respectively for (a) observation, (b) AMIP, (c) CMIP and (d) AMIP-CMIP_SST. Contour interval is 0.1. The absolute value more than 0.2 is above 95% confidence level.

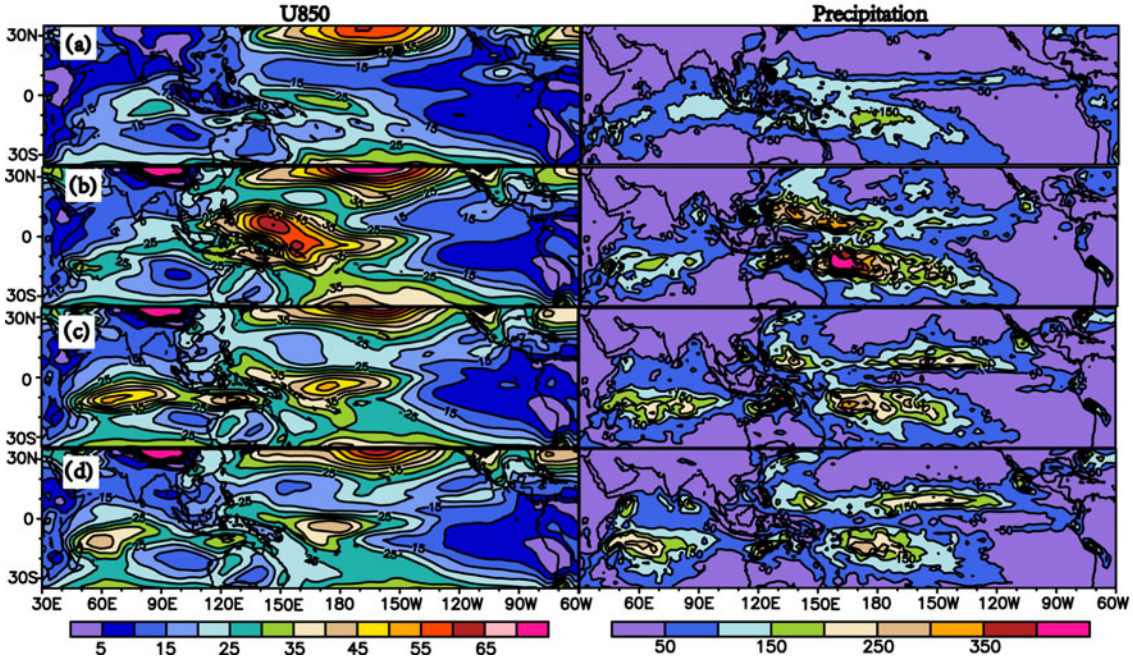

Fig. 6. 20–100-day band-pass filtered precipitation variance (left panel) and U850 variance (right panel) during boreal winter, respectively for (a) observation data, (b) AMIP, (c) CMIP, and (d) AMIP-CMIP_SST. Units for precipitation variance are $mm^2\ d^{-2}$; units for zonal wind variance are $m^2\ s^{-2}$.

than that in AMIP.

During summer, the U850 and precipitation variance maxima were located over the eastern Indian Ocean, the Asian monsoon region, and the eastern tropical Pacific according to the observation data (Fig. 7a). These major centers of variances were captured in AMIP, but their amplitude was obviously overestimated particularly in the Asian monsoon region (Fig. 7b). The overestimated amplitude in AMIP was evidently reduced in CMIP over the Asian monsoon region (Fig. 7c). However, the amplitude of variance over the Indian Ocean was enhanced, and the location of variance maxima over the Indian Ocean shifted southwestward in CMIP (Fig. 7c). CMIP and AMIP, shared a common disadvantage, that is, the unrealistic split of maximum TISO precipitation variance over the Pacific (Figs. 7b and c).

4. Discussion

We investigated the possible reasons for the differences in the simulated TISOs between AMIP and CMIP in the following two aspects: the mean state and atmosphere–ocean coupling. To clarify the respective roles of the mean state and atmosphere–ocean coupling on TISO simulation, we conducted another AMIP-type experiment forced by monthly SSTs after atmosphere–ocean coupling (the output monthly SST in CMIP run), called "AMIP-CMIP_SST" hereafter.

4.1 *Associated with mean state*

On one hand, some previous studies have shown that the biases in the simulated TISO/MJO are related to biases in their embedding mean state (e.g., Slingo et al., 1996; Zhang et al., 2006; Ajayamohan and Goswami, 2007; Yang et al., 2009). On the other hand, some studies have reported that the good mean states do not necessarily lead to good TISO simulations (e.g., Rajendran et al., 2008; Liu et al., 2009). Then, what are the relationships between the mean state and the TISO activity in SAMIL? To remove the impact of atmosphere–ocean coupling, we first compared the differences between AMIP and AMP-CMIP_SST to identify the role of the mean state on TISO.

First, Fig. 8 shows the difference of seasonal mean SSTs between two experiments (AMIP and AMIP-CMIP_SST). The SST after atmosphere–ocean coupling exhibited the obvious cooling biases over Asian-Australian monsoon region (AAM; the Arabian Sea, the Bay of Bengal, the South China Sea, the Maritime continent, and the western North Pacific). In contrast, the SST over the equatorial and the southern Indian Ocean had warming biases. Physically speaking, warming SST enhanced rainfall, while cooling SST depressed rainfall without the feedback from atmosphere to ocean. Therefore, there was correspondingly less precipitation over the AAM region and more precipitation over the southern Indian Ocean in AMIP-CMIP_SST than in AMIP (Figs. 9b and d). In comparison with the observation data, the precipitation in AMIP was overestimated over the AAM region and the tropical southern Indian Ocean (Figs. 9a and b), so that the biases of the precipitation mean state were obviously reduced over the AAM region but were increased over the southern Indian Ocean in AMIP-CMIP_SST. Accordingly, we found that the intensity of simulated TISO activity was more realistic over the AAM region but was overestimated over the southern Indian Ocean in AMIP_CMIP-SST than in AMIP (Figs. 6 and 7).

Inness et al. (2003) suggested that a correct mean low-level zonal wind in a model is critical to its TISO simulation, because the observed maximum TISO activity (variance) tends to be located in regions of either westerlies or very weak easterlies at 850 hPa (Figs. 6, 7, and 10a). Figure 10b shows that the tropical westerly intensity in AMIP was overestimated over the Maritime continent, was underestimated over the Indian Ocean during winter, and was overestimated over the AAM region during summer. These biases in AMIP were obviously reduced in AMIP-CMIP_SST (Fig. 10d). Correspondingly, we found that better variance distribution of TISO was reproduced over these regions in AMIP_CMIP-SST (Figs. 6d and 7d), which is consistent with the results of Inness et al. (2003).

The above analysis indicates a tentative conclusion that a better mean state means a better TISO intensity. Does a better mean state cause better depiction of characteristics of TISO activity? We further compared the power spectrum, the wavenumber–frequency spectra, and the propagations of TISO between AMIP and AMIP-CMIP_SST (Figs. 1–5). Although the 30–80-day eastward propagating spectrum peaks during winter, the Kelvin wave is a symmetric component and the MRW is an asymmetric component in wave-number frequency spectrum analysis. The eastward propagation over the western Pacific Ocean during winter was better in AMIP-CMIP_SST, most TISO activity biases were not reduced under better mean state, and some biases were even increased (e.g., the power spectrum during summer). Therefore, a better mean state does not necessarily cause a better depiction of features of TISO itself.

The comparison between AMIP and AMIP-CMIP_SST also indicated that the stronger TISO signal in precipitation appeared to be collocated with

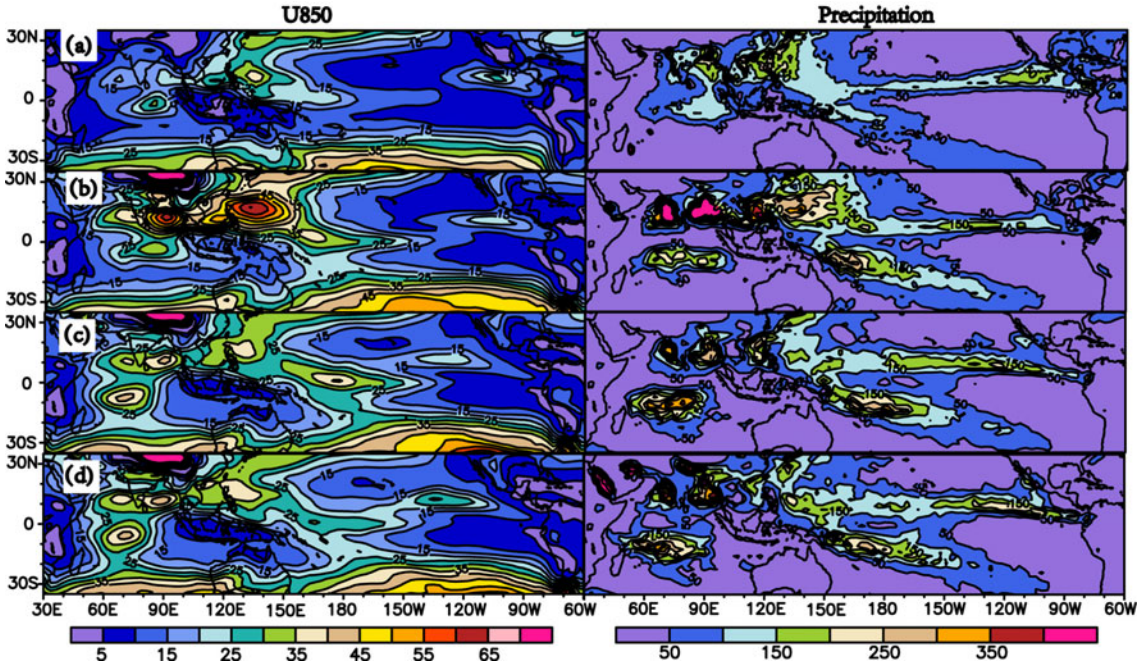

Fig. 7. Same as Fig. 5 except for the boreal summer.

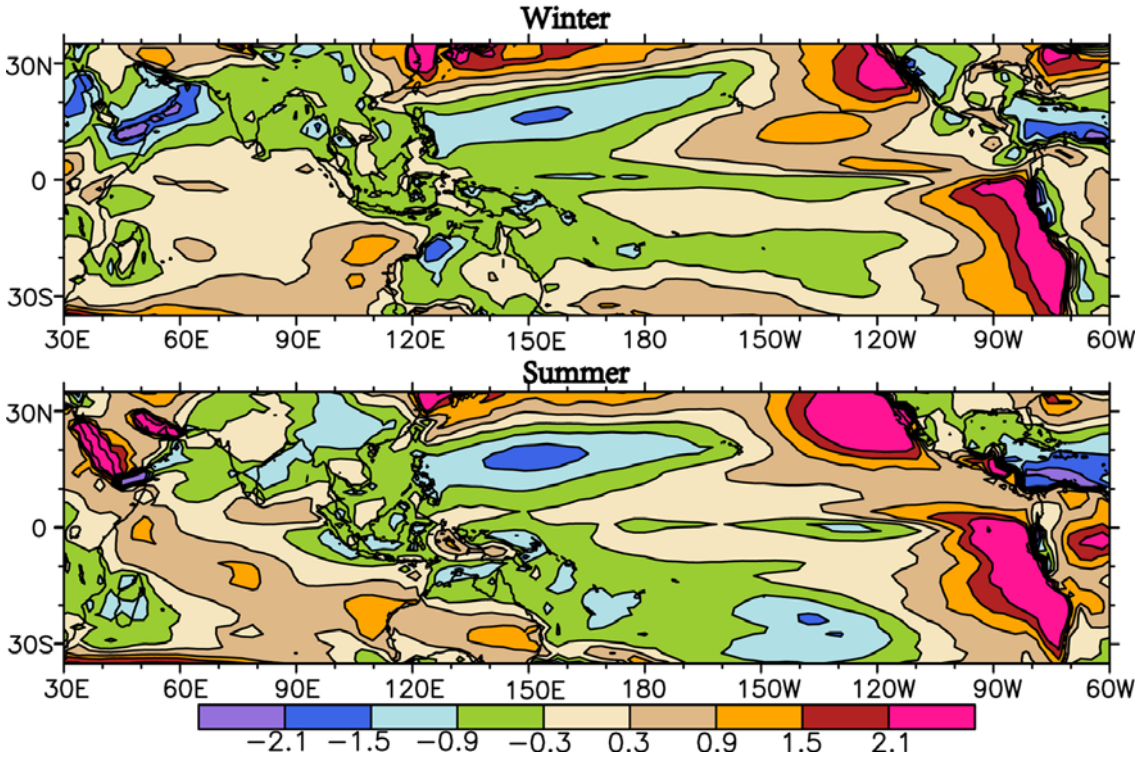

Fig. 8. Seasonal mean differences of SST between AMIP and AMIP-CMIP_SST runs (AMIP-CMIP_SST run minus AMIP run) respectively during winter (upper panel) and summer (lower panel). The units are degrees.

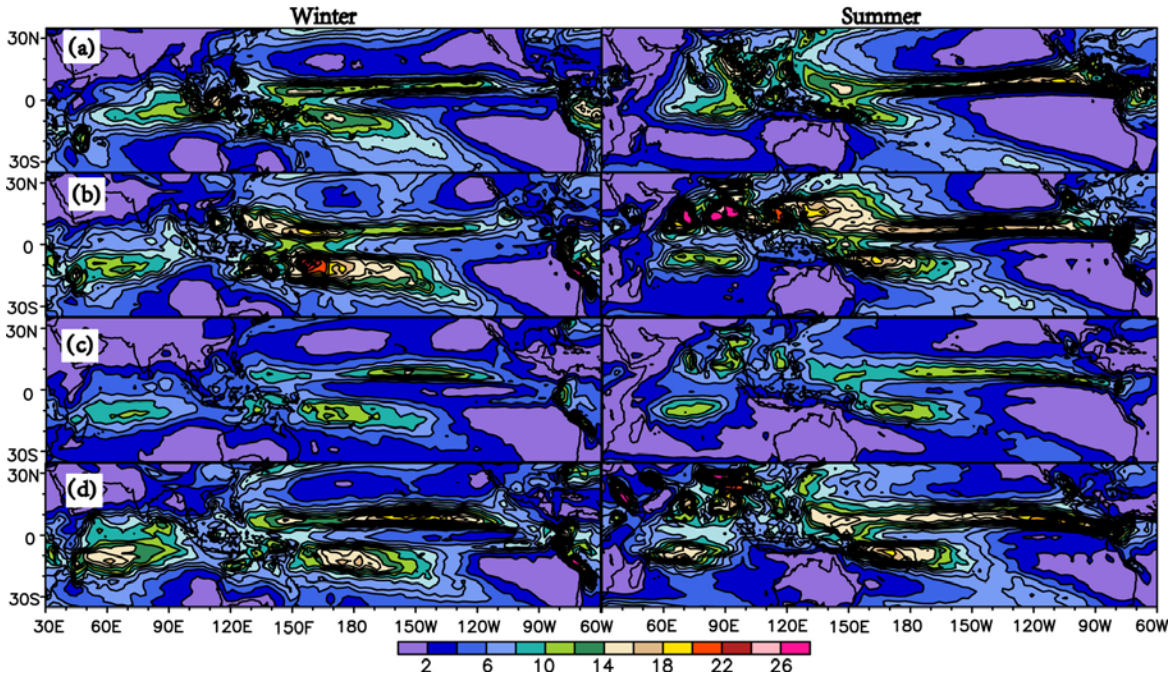

Fig. 9. Climatological mean precipitation during winter (left panel) and summer (right panel) in 11 years, respectively for (a) observation data, (b) AMIP, (c) CMIP, and (d) AMIP-CMIP_SST. Units: mm d^{-1}.

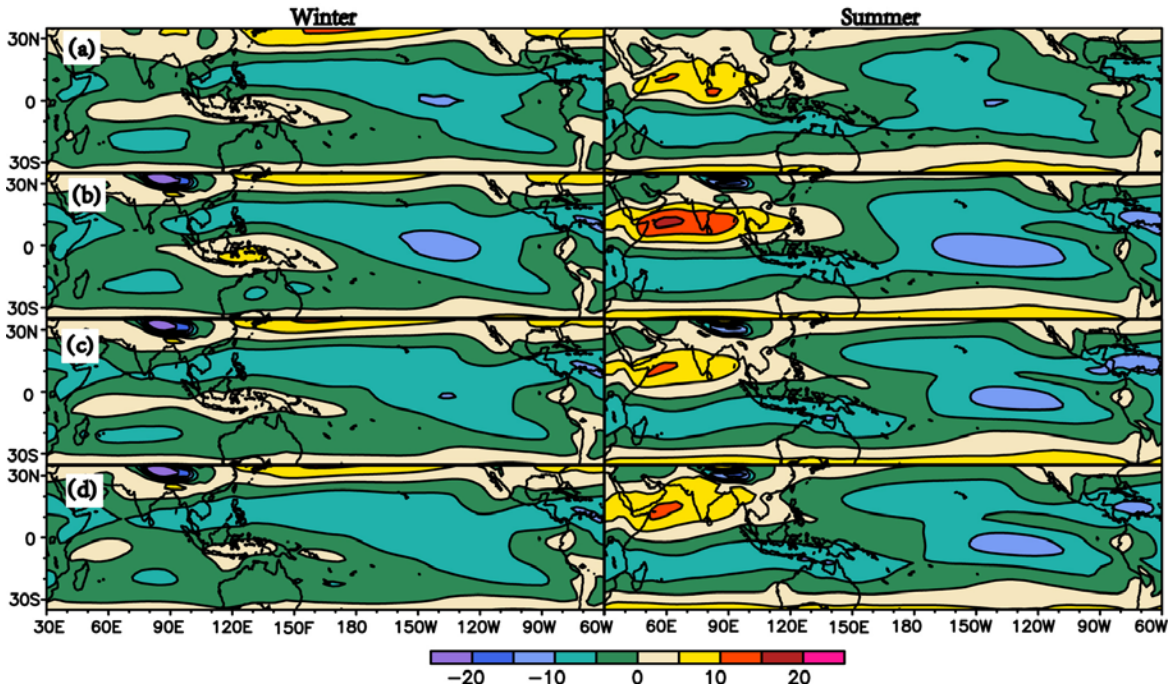

Fig. 10. Same as Fig. 7, except for U850. Units: m s^{-1}.

mean precipitation with the larger amplitude (Figs. 6, 7, and 9). The unrealistic split of maximum TISO precipitation over the western Pacific Ocean in both experiments appeared to be related to the exaggeration of the double-ITCZ structure in mean precipitation. However, this is not always true when comparing AMIP-CMIP_SST and CMIP. For example, the precipitation over the western north Pacific had smaller amplitude in the mean state of CMIP than in AMIP-CMIP_SST during winter (Fig. 9), but it had stronger TISO activity in CMIP than in AMIP-CMIP_SST (Fig. 6).

4.2 *Associated with atmosphere–ocean interaction*

Compared with both AMIP and AMIP-CMIP_SST, TISO activity in CMIP was evidently improved in some aspects, including the realistic eastward propagation over the western Pacific Ocean and the stronger power spectrum of 30–80-day eastward periods (Figs. 1, 2 and Fig. 4). These improvements resulted directly from atmosphere–ocean coupling. The lagged-time-longitude diagram between 20–100-day filtered SST and precipitation along the equator upon the 20–100-day filtered precipitation over the Indian Ocean reference region are shown in Fig. 11. We found that the simulated 20–100-day filtered precipitation and SST anomalies were in quadrature in the coupled run, with the warm SST anomaly leading the wet anomaly, which has been found in the observation data (e.g., Waliser et al., 1999; Matthews, 2004; Wang et al., 2006). The presence of positive SST anomalies enhances the initial low-level convergence that subsequently extends up to the mid-troposphere and causes deep convection. However, in the two uncoupled runs (AGCM runs), the realistic relationship between the 20–100-day filtered precipitation and SST almost disappeared, indicating that the convection in uncoupled run was subjected to the given SST instead of its evolution through coherent coupled feedback.

However, the simulations of eastward propagation in winter over the Indian Ocean were still very poor in both the CMIP and the AMIP. This error has been identified as one of the major problems in simulating intraseasonal oscillations (Waliser et al., 2003). The mean precipitation maxima over the equatorial central Indian Ocean unrealistically shifted southwestward the Southern Hemisphere (Fig. 9), which may have contributed to the biases of the eastward propagation over the Indian Ocean in simulation.

Inconsistent with many previous findings that show atmosphere–ocean interaction enhances the northward propagation of TISO during summer, the northward propagation was not improved in CMIP (Fig. 5). To investigate the cause of this difference, we first chose some strong TISO cases with the longer periods (>30 days) in CMIP to determine its evolution (the year-by-year time series of 20–100-day in 11 years are not shown here), and we found that the northward propagation of 20–100-day TISO was well distinguished in some cases (e.g., 15 May to 16 Jun 1992) (Fig. 12). The

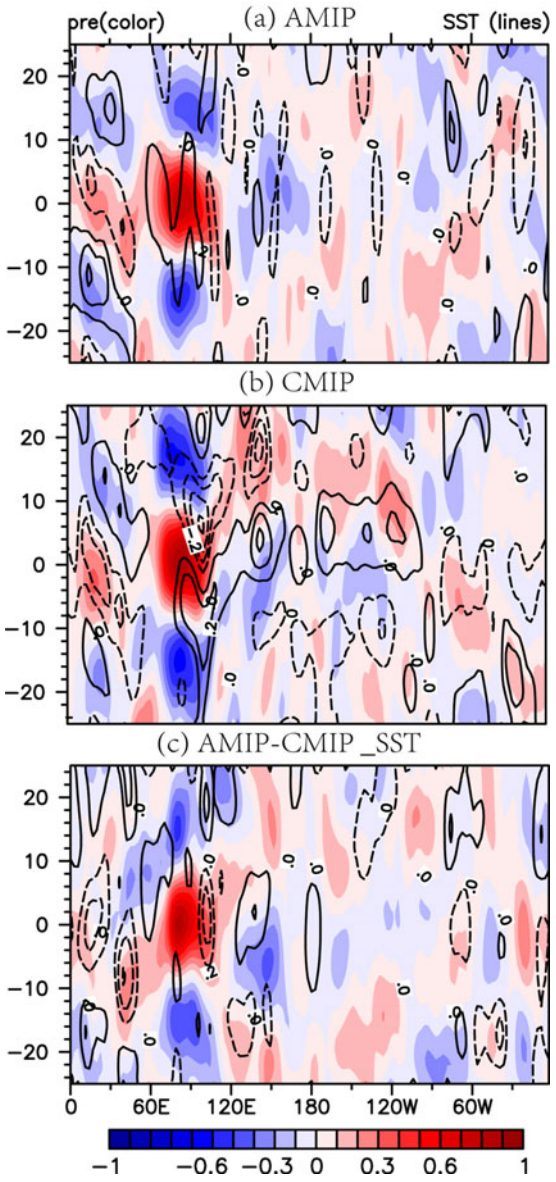

Fig. 11. Lagged-time-longitude diagram of correlation coefficients between 20–100-day filtered precipitation (color shading) and SST (contours) over 10°S–10°N during boreal winter against to 20–100-day filtered precipitation over the reference region (10°S–5°N and 75°–100°E), respectively in (a) AMIP, (b) CMIP, and (c) AMIP-CMIP_SST. The contour interval is 0.1. The absolute value > 0.2 is above the 95% confidence level.

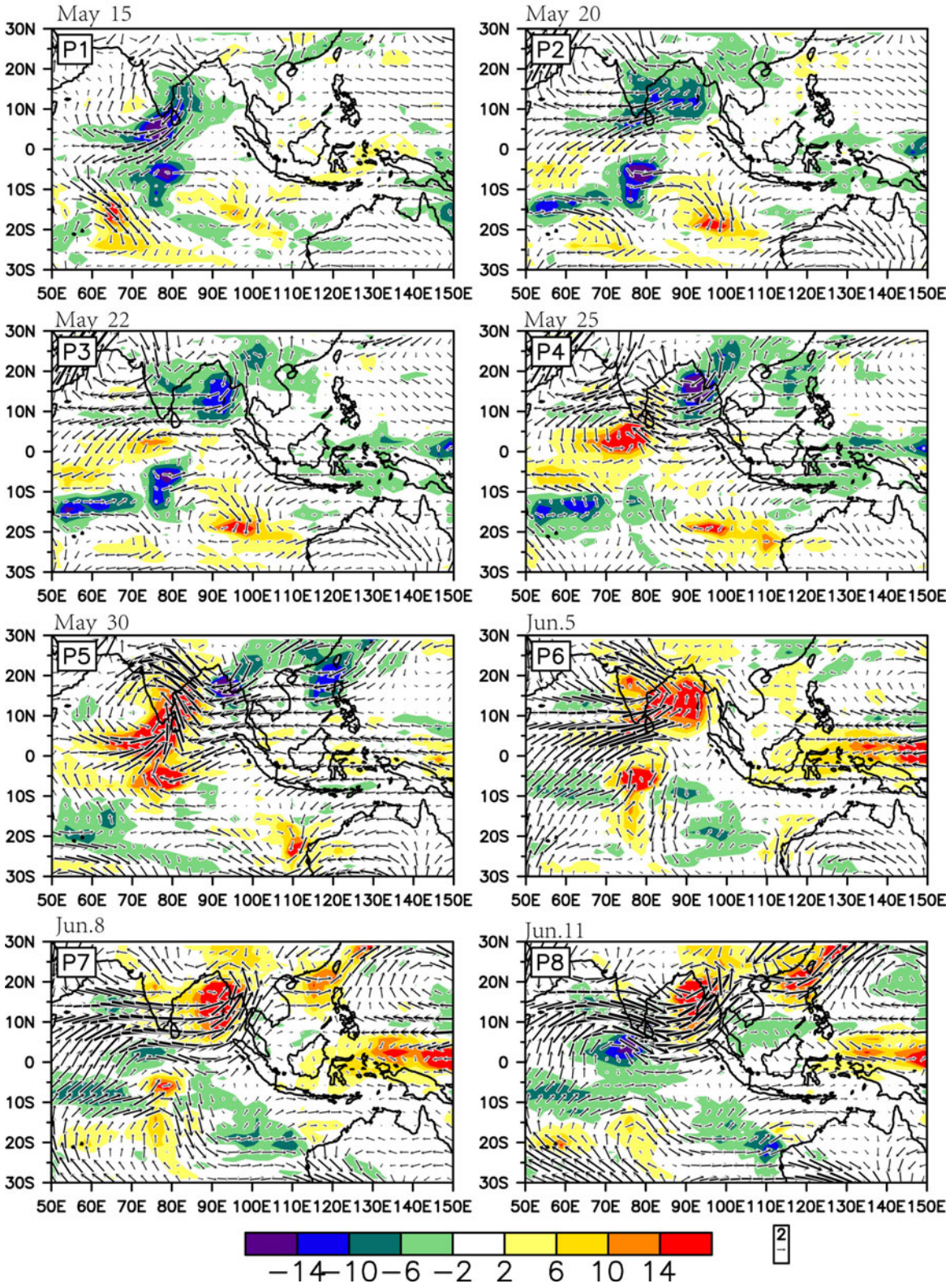

Fig. 12. Evolution of 20–100-day filtered precipitation (shading) and 850-hPa wind (vector) in a strong TISO case during 1992 summer in CMIP run. Units for precipitation are mm d^{-1}; units for wind are m s^{-1}.

phase-leading relationship between SSTA and precipitation was also seen in the case study (figure not shown). Again, we chose some weak cases of TISO with the shorter periods (20–30 days) in CMIP, and we found that the northward propagation of 20–100-day TISO almost disappeared and the unrealistic southward propagation occurred (figure not shown). This is why the averaged lagged-time-latitude correlation analysis did not show remarkable improvement in the simulation of northward propagation in CMIP. The results from case-by-case studies indicated the following three points: (1) the averaged lagged-time-latitude correlation analysis in MJOWG diagnostic package was not necessarily able to well represent the boreal summer TISO (also called BSISO), particularly the northward propagation; (2) the 20–100-day band filtering might be too broad for the summer ISO, which might involve different types of transient activity with different periodicities; (3) the atmosphere–ocean coupling was able to enhance the northward propagation during summer in some strong TISO cases in this study, which is still consistent with previous findings.

5. Summary

This study comprehensively evaluated the performance of TISO during winter and summer in uncoupled (AMIP) and coupled (CMIP) simulations of SAMIL. In the power spectrum, the AMIP was realistically able to capture the zonal wavenumbers 1–3 of precipitation and the zonal wave number 1 of U850 in eastward propagating power, but it failed to simulate the 30–80-day peak during eastward periods, and it overestimated the power spectrum during westward periods. In contrast, the CMIP obviously intensified the spectral peak of 30–80-day eastward periods and strengthened the eastward propagating power relative to the westward propagating signals. Meanwhile, the CMIP showed stronger signals of Kelvin waves and MRG waves. In propagation, the AMIP was able to capture well the eastward propagation over the western Pacific Ocean but failed over the Indian Ocean in winter, and the AMIP was able to reproduce the eastward propagation to some extent over the Indian Ocean portion but failed over the western Pacific Ocean in summer. The CMIP evidently strengthened the eastward propagating signals in the western Pacific Ocean during both summer and winter. However, both AMIP and CMIP failed to give realistic results for northward propagation over the Indian Ocean. In spatial distribution, CMIP showed a more realistic location and intensity of TISO variance maxima than AMIP in winter; during summer, the errors of the variance amplitude in AMIP were obviously reduced in CMIP over the Asian monsoon region, but the biases of the TISO variance over the Indian Ocean were enlarged in CMIP. The unrealistic split of maximum 20–100-day filtered precipitation variance over Pacific is a common disadvantage in both CMIP and AMIP.

To clarify the respective impact of mean state and the atmosphere–ocean coupling on TISO simulation, we conducted one more AGCM experiment (called AMIP-CMIP_SST) forced by CMIP output monthly SST. The comparison between AMIP and AMIP-CMIP_SST indicates the relationship between the mean state and TISO activity in the following aspects. First, better 850-hPa westerlies corresponded to better distributions of TISO intensity because the maximum TISO variance tended be located in regions of the lower-level westerlies. Second, stronger precipitation mean state usually led to stronger TISO activity, but this did not always hold true. Third, a better mean state does not necessarily mean better features of TISO itself (e.g., power spectrum and propagation).

The comparison of CMIP and AMIP-CMIP_SST and AMIP showed that atmosphere–ocean coupling evidently improved the eastward propagation over the western Pacific Ocean and the 30–80-day eastward propagating power spectrum by better capturing a realistic relationship between precipitation and SST, but it failed to improve the northward propagation in mean lagged-time-latitude diagram of correlation coefficients. However, case studies showed that the northward propagation could be reproduced realistically in some strong TISO cases in the coupled run. The inconsistency between the case study and the averaged lagged-time-latitude correlation analysis indicates that this diagnostic package of MJOWG may not represent well the summer ISO (i.e., the 20–100-day band filter might be too wide for the summer ISO).

The failure to capture the eastward propagation during winter over the Indian Ocean is assumed to be associated with the biases of rainfall simulation over the equatorial central Indian Ocean in both CMIP and AMIP runs. The causes for the unrealistic mean state simulation over the equatorial central Indian Ocean need to be clarified in a future study. More improvement might be made in the physical package, including convective parameterization and cloud scheme.

Acknowledgements. This study was supported by "863" program (Grant No. 2010AA012305), "973" program (Grant Nos. 2012CB955401, 2010CB950404 and 2012CB417203), the specialized Research Fund for the Doctoral Program of Higher Education (SRFDP), the National Natural Science Foundation of China (Grant No. 41005036), and the State Key Laboratory of Earth Surface Processes and Resource Ecology (Grant No. 2010ZY03).

REFERENCES

Ajayamohan, R. S., and B. N. Goswami, 2007: Dependence of simulation of summer tropical intraseasonal oscillations on the simulation of seasonal mean. *J. Atmos. Sci.,* **64**, 460–478.

Bao, Q., G. Wu, Y. Liu, J. Yang, Z. Wang, and T. Zhou, 2010: An introduction to the coupled model FGOALS1.1-s and its performance in East Asia. *Adv. Atmos. Sci.,* **27**, 1131–1142.

Bergman, J. W., H. H. Hendon, and K. M. Weickmann, 2001: Intraseasonal air-sea interactions at the onset of El Niño. *J. Climate*, **14**, 1702–1719.

Brinkop, S., and E. Roeckner, 1995: Sensitivity of a general-circulation model to parameterizations of cloud-turbulence interactions in the atmospheric boundary-layer. *Tellus*(A), **47**, 197–220.

Duchon, C. E., 1979: Lanczos filtering in one and two dimensions. *J. Appl. Meteor.,* **18**, 1016–1022.

Edwards, J. M., and A. Slingo, 1996: A studies with a flexible new radiation code. I: Choosing a configuration for a large-scale model. *Quart. J. Roy. Meteor. Soc.*, **122**, 689–720.

Fu, X., and B. Wang, 2004: Different solutions of intraseasonal oscillation exist in atmosphere ocean coupled model and atmosphere-only model. *J. Climate,* **17**, 1263–1271.

Fu, X., and B. Wang, 2009: Critical roles of the stratiform rainfall in sustaining the Madden–Julian oscillation: GCM experiments. *J. Climate*, **22**, 3939–3959.

Hayashi, Y., 1979: A generalized method of resolving transient disturbances into standing and traveling waves by space-time spectral analysis. *J. Atmos. Sci.,* **36**, 1017–1029.

Hayashi, Y., and D. G. Golder, 1986: Tropical intraseasonal oscillations appearing in a GFDL general circulation model and FGGE data. Part I: Phase propagation. *J. Atmos. Sci.,* **43**, 3058–3067.

Hendon, H. H., 2000: Impact of air-sea coupling on the Madden-Julian Oscillation in a general circulation model. *J. Atmos. Sci.*, **57**, 3939–3952.

Hendon, H. H., and B. Liebmann, 1990: The intraseasonal (30–50 day) oscillation of the Australian summer monsoon. *J. Atmos. Sci.*, **47**, 2909–2924.

Higgins, R. W., and W. Shi, 2001: Intercomparison of the principal modes of interannual and intraseasonal variability of the North American monsoon system. *J. Climate*, **14**, 403–417.

Huffman, G. J., and Coauthors, 2001: Global precipitation at one-degree daily resolution from multisatellite observations. *J. Hydrometeor.*, **2**, 36–50.

Inness, P. M., J. M. Slingo, E. Guilyardi, and J. Cole, 2003: Simulation of the Madden-Julian oscillation in a coupled general circulation model. Part II: The role of the basic state. *J. Climate*, **16**, 365–382.

Jiang, X., and Coauthors, 2009: Vertical heating structures associated with the MJO as characterized by TRMM estimates, ECMWF reanalyses, and forecasts: A case study during 1998/99 winter. *J. Climate*, **22**, 6001–6020.

Kalnay, E., and Coauthors, 1996: The NCEP/NCAR 40-year reanalysis project. *Bull. Amer. Meteor. Soc.*, **77**, 437–471.

Kessler, W. S., and R. Kleeman, 2000: Rectification of the Madden-Julian oscillation into the ENSO cycle. *J. Climate*, **13**, 3560–3575.

Kiladis, G. N., and K. M. Weickmann, 1992: Circulation anomalies associated with tropical convection during northern winter. *Mon. Wea. Rev.*, **120**, 1900–1923.

Kim, D., and Coauthors, 2009: Application of MJO simulation diagnostics to climate models. *J. Climate*, **22**, 6413–6436.

Krishnamurti, T. N., and D. Subrahmanyam, 1982: The 30–50-day mode at 850 mb during MONEX. *J. Atmos. Sci.,* **39**, 2088–2095.

Lau, K. M., and P. H. Chan, 1986: Aspects of the 40–50 day oscillation during the northern summer as inferred from outgoing longwave radiation. *Mon. Wea. Rev.*, **114**, 1354–1367.

Lau, K. M., L. M. Held and J. D. Neelin, 1988: The Madden-Julian oscillation in an idealized general circulation model. *J. Atmos. Sci.,* **45**, 3810–3832.

Li, C., X. L. Jia, J. Ling, W. Zhou, and C. D. Zhang, 2009: Sensitivity of MJO simulations to diabatic heating profiles. *Climate Dyn.,* **32**, 167–187.

Liebmann, B., and D. L. Hartmann, 1984: An observational study of tropical-midlatitude interaction on intraseasonal time scales during winter. *J. Atmos. Sci.*, **41**, 3333–3350.

Liebmann, B., H. H. Hendon, and J. D. Glick, 1994: The relationship between tropical cyclones of the western Pacific and Indian Oceans and the Madden–Julian oscillation. *J. Meteor. Soc. Japan*, **72**, 401–411.

Liu, H., and G. X. Wu, 1997: Impacts of land surface on climate of July and onset of summer monsoon: A study with an AGCM plus SSiB. *Adv. Atmos. Sci.*, **14**, 289–308.

Liu, H. L., X. Zhang, W. Li, Y. X. Yu, and R. C. Yu, 2004: An eddy-permitting oceanic general circulation model and its preliminary evaluations. *Adv. Atmos. Sci.*, **21**, 675–690.

Liu, P., and Coauthors, 2009: Tropical intraseasonal variability in the MRI-20km60L AGCM. *J. Climate*, **22**, 2006–2022.

Madden, R. A., and P. R. Julian, 1971: Detection of a 40–50 day oscillation in the zonal wind in the tropical Pacific. *J. Atmos. Sci.*, **28**, 702–708.

Madden, R. A., and P. R. Julian, 1972: Description of global-scale circulation cells in the Tropics with a 40–50 day period. *J. Atmos. Sci.,* **29**, 1109–1123.

Maloney, E. D., and D. L. Hartmann, 2000: Modulation of eastern North Pacific hurricanes by the Madden-Julian oscillation. *J. Climate*, **13**, 1451–1460.

Matthews, A. J., 2004: Atmospheric response to observed intraseasonal tropical sea surface temperature anomalies. *Geophys. Res. Lett.,* **31**, L14107, doi: 10.1029/2004GL020474.

Murakami, T., T. Nakazawa, and J. He, 1984: On the 40–

50 day oscillations during the 1979 northern hemisphere summer. I: Phase propagation. *J. Meteor. Soc. Japan,* **62**, 440–468.

Nordeng, T. E., 1994: Extended versions of the convective parameterization scheme at ECMWF and their impact on the mean and transient activity of the model in the tropics. *ECMWF Technical Memo.* 206, Reading, England, 41pp.

Palmer, T. N., G. J. Shutts, and R. Swinbank, 1986: Alleviation of a systematic westerly bias in general circulation and numerical weather prediction models through an orographic gravity wave drag parameterization. *Quart. J. Roy. Meteor. Soc.,* **112**, 1001–1039.

Pan, L. L., and T. Li, 2008: Interactions between the tropical ISO and midlatitude low-frequency flow. *Climate Dyn.*, **31**, 375–388.

Rajendran, K., A. Kitoh, R. Mizuta, S. Sajani, and T. Nakazawa, 2008: High-resolution simulation of mean convection and its intraseasonal variability over the Tropics in the MRI/JMA 20-km mesh AGCM. *J. Climate*, **21**, 3722–3739.

Slingo, J. M., and Coauthors, 1996: Intraseasonal oscillations in 15 atmospheric general circulation models: Results from an AMIP diagnostic subproject. *Climate Dyn.*, **12**, 325–357.

Song, X. L., 2005: The evaluation analysis of two kinds of mass flux cumulus parameterizations in climate simulation. Ph. D. dissertation, Institute of Atmospheric Physics, Chinese Academy of Sciences, 119–145. (in Chinese)

Sperber, K. R., J. M. Slingo, P. M. Inness, and K. M. Lau, 1997: On the maintenance and initiation of the intraseasonal oscillation in the NCEP/NCAR reanalysis and the GLA and UKMO AMIP simulations. *Climate Dyn.,* **13**, 769–79.

Sperber, K. R., S. Gualdi, S. Legutke, and V. Gayler, 2005: The Madden-Julian oscillation in ECHAM4 coupled and uncoupled general circulation models. *Climate Dyn.*, **25**, 117–140.

Sun, Z., and L. Rikus, 1999a: Improved application of ESFT to inhomogeneous atmosphere. *J. Geophys. Res.,* **104**, 6291–6303.

Sun, Z., and L. Rikus, 1999b: Parameterization of effective radius of cirrus clouds and its verification against observations. *Quart. J. Roy. Meteor. Soc.*, **125**, 3037–3056.

Takayabu, Y. N., T. Iguchi, M. Kachi, A. Shibata, and H. Kanzawa, 1999: Abrupt termination of the 1997–98 El Niño in response to a Madden-Julian oscillation. *Nature*, **402**, 279–282.

Taylor, K. E., R. J. Stouffer, and G. A. Meehl, 2009: A summary of the CMIP5 experiment design. [Available online from http://cmip-pcmdi.llnl.gov/cmip5/docs/Taylor_CMIP5_design.pdf]

Tian, B. J., Y. L. Yung, D. E. Waliser, T. Tyranowski, L. Kuai, E. J. Fetzer, and F. W. Irion, 2007: Intraseasonal variations of the tropical total ozone and their connection to the Madden-Julian Oscillation. *Geophys. Res. Lett.*, **34**, L08704, doi: 10.1029/2007GL029451.

Tian, B. J., and Coauthors, 2008: Does the Madden-Julian oscillation influence aerosol variability? *J. Geophys. Res.*, **113**, D12215, doi: 10.1029/2007JD009372.

Tiedtke, M., 1989: A comprehensive mass flux scheme for cumulus parameterization in large-scale models. *Mon. Wea. Rev.,* **117**, 1779–1800.

Tokioka, T., K. Yamazaki, A. Kitoh, and T. Ose, 1988: The equatorial 30–60 day oscillation and the Arakawa-Schubert penetrative cumulus parameterization. *J. Meteor. Soc. Japan*, **66**, 883–901.

Waliser, D. E., and Coauthors, 2003: AGCM simulations of intraseasonal variability associated with the Asian summer monsoon. *Climate Dyn.*, **21**, 423–446.

Waliser, D. E., K. M. Lau, J. H. Kim, 1999: The influence of coupled sea surface temperatures on the Madden–Julian oscillation: a model perturbation experiment. *J. Atmos. Sci.,* **56**, 333–358.

Waliser, D. E., R. Murtugudde, P. Strutton, and J.-L. Li, 2005: Subseasonal organization of ocean chlorophyll: Prospects for prediction based on the Madden-Julian oscillation. *Geophys. Res. Lett.*, L23602, doi: 10.1029/2005GL024300.

Waliser, D. E., and Coauthors, 2009: MJO simulation diagnostics. *J. Climate*, **22**, 3006–3030.

Wang, B., 2005: Theories. *Intraseasonal Variability of the Atmosphere-Ocean Climate System,* Lau and Waliser, Eds., Springer-Verlag, Heidelberg, Germany, 436pp.

Wang, B., and H. Rui, 1990: Synoptic climatology of transient tropical intraseasonal convection anomalies—1975–1985. *Meteor. Atmos. Phys.*, **44**, 43–61.

Wang, B., P. Webster, K. Kikuchi, T. Yasunari, and Y. Qi, 2006: Summer quasi-monthly oscillation in the global tropics. *Climate Dyn.,* **27**, 661–675.

Wang, B., and X. Xie, 1997: A model for the summer intraseasonal oscillation. *J. Atmos. Sci.,* **54**, 72–86.

Wang, B., and X. Xie, 1998: Coupled modes of the warm pool climate system. Part I: The role of air–sea interaction in maintaining Madden–Julian oscillations. *J. Climate*, **8**, 2116–2135.

Wang, W. Q., and M. E. Schlesinger, 1999: The dependence on convection parameterization of the tropical intraseasonal oscillation simulated by the UIUC 11-layer atmospheric GCM. *J. Climate*, **12**, 1423–1457.

Weickmann, K. M., 1983: Intraseasonal circulation and outgoing longwave radiation modes during northern hemisphere winter. *Mon. Wea. Rev.*, **111**, 1838–1858.

Weickmann, K. M., G. R. Lussky, and J. E. Kutzbach, 1985: Intraseasonal (30–60 Day) fluctuations of Outgoing Longwave Radiation and 250 mb streamfunction during northern winter. *Mon. Wea. Rev.*, **113**, 941–961.

Wheeler, M., and G. N. Kiladis, 1999: Convectively coupled equatorial waves: analysis of clouds and temperature in the wavenumber–frequency domain. *J. Atmos. Sci.*, **56**, 374–399.

Yang, J., B. Wang, and B. Wang, 2008: Anticorrelated intensity change of the quasi-biweekly and 30–50 day oscillations over the South China Sea. *Geophys. Res. Lett.,* doi: 10. 1029/2008GL034449.

Yang, J., B. Wang, B. Wang, and L. J. Li, 2009: The East Asia-western North Pacific summer intraseasonal oscillation simulated in GAMIL 1.1.1. *Adv. Atmos. Sci.,* **26**, 480–492, doi: 10.1007/s00376-009-0480-7.

Yasunari, T., 1979: Cloudiness fluctuations associated with the northern hemisphere summer monsoon. *J. Meteor. Soc. Japan*, **57**, 227–242.

Zhang, C., M. Dong, H. H. Hendon, E. D. Maloney, A. Marshall, K. R. Sperber, and W. Wang, 2006: Simulations of the Madden-Julian oscillation in four pairs of coupled and uncoupled global models. *Climate Dyn.*, doi: 10.1007/s00382-006-0148-2.

Zhang, G. J., and X. Song, 2009: Interaction of deep and shallow convection is key to Madden-Julian oscillation simulation. *Geophys. Res. Lett.,* **36,** L09708, doi: 10.1029/2009GL037340.

Zhou, W., and J. C. Chan, 2005: Intraseasonal oscillations and the South China Sea summer monsoon onset. *Int. J. C1imatol*, **25**, 1585–1609.